Disclaimer

This note has not been internally reviewed by the DØ Collaboration. Results or plots contained in this note were only intended for internal documentation by the authors of the note and they are not approved as scientific results by either the authors or the DØ Collaboration. All approved scientific results of the DØ Collaboration have been published as internally reviewed Conference Notes or in peer reviewed journals.

DØ note # 2136
May 24, 1994

Recent QCD Results from CDF and DØ

Jianming Qian
Department of Physics
The University of Michigan
Ann Arbor, Michigan 48109

Presented at the XXIXth Recontres de Moriond
QCD and High Energy Hadron Interactions
Meribel, France
March 19-26, 1994

ABSTRACT

Both the CDF and DØ detectors at the Tevatron $\bar{p}p$ collider have accumulated a large sample of events with jets in the final state. The large statistics enables detailed studies of dijet and multijet final states. Recent results about the dijet angular distributions, dijet differential cross sections, dijet production for different rapidity intervals and properties of multijet events are described. The data are compared with leading-order or next-to-leading-order QCD calculations, or with the predictions of parton shower based Monte Carlo models. For most of the variables studied, good agreement is observed between the data and the QCD calculations or between the data and the model predictions. Finally, the fraction of events with an observed rapidity gap measured by DØ is reported.

1 Introduction

The Fermilab Tevatron collider provides an unique opportunity to study the properties of hard interactions in $\bar{p}p$ collisions at short distances. The hard scattering is described by the theory of perturbative Quantum ChromoDynamics (QCD) [1] and has been studied extensively in the last decade. Within the context of QCD, the hard process is described as the point-like scattering between constituent partons (quarks and gluons) of protons and anti-protons, convoluted with parton momentum distributions inside the nucleon. Colored partons from hard scattering undergo soft quark and gluon radiation and the hadronization process to form detectable colorless hadrons, which appear in the detector as localized energy deposits identified as jets. Jets originating from partons in the initial hard scattering process are typically isolated from other collision products and have large transverse energies. They preserve the energy and direction of the initial partons. Therefore, the properties of the final jet system are directly related to those of the initial parton system.

The CDF detector recorded a data sample corresponding to an integrated luminosity of 19 pb^{-1} during the 1992-93 Tevatron run. The DØ experiment was commissioned during the spring of 1992 and accumulated a total luminosity of 16 pb^{-1} in its initial run. This paper presents some of the preliminary results on dijet, multijet and rapidity gap physics from the two experiments. Both CDF and DØ detectors are able to measure jet final states. With its uniform, hermetic and large coverage calorimetry, the DØ detector is especially suited for studying jet final states. The detailed description of the two detectors can be found in [2].

The jets are reconstructed using a fixed cone jet algorithm [3] in (η, ϕ) space. The algorithm assigns all energy within a cone of $\Delta R = \sqrt{\Delta^2\eta + \Delta^2\phi} = 0.7$ around an initial seed cluster to the jet. Both collider and test-beam data are used in determining jet energy scale. CDF uses momentum measurements of isolated charged tracks of the collider data by the tracking chamber to calibrate the jet energy while in DØ the jet energy scale is tied to the electromagnetic energy scale by balancing the transverse energies of the direct photon candidate events.

2 Dijet Final State

Within the context of QCD, the leading-order (LO) $\mathcal{O}(\alpha_s^2)$ is easily calculable. A dijet final state is the simplest QCD process of $\bar{p}p$ collision. The next-to-leading-order (NLO) $\mathcal{O}(\alpha_s^3)$ calculations are technically difficult and are only available recently for a limited number of variables. The advantage of the NLO calculations over LO calculations is that the results are less sensitive to the choice of renormalization scale. Unless otherwise quoted, all theoretical calculations described in this paper are evaluated at the scale $E_T/2$. In the following, the dijet angular distributions, dijet differential cross sections, and dijet production for different rapidity intervals are presented. The dijet events used for these studies are inclusive events. The two highest E_T jets are used in the analyses and any additional jets are ignored.

2.1 Dijet Angular Distributions

The dijet angular distributions are measured for events with two or more jets. In the center-of-mass system (CMS) of the two jets with highest E_T, the dijet kinematics are completely determined by the scattering angle $\cos\theta^*$ and dijet mass M_{jj}. The dominance of vector gluon exchange gives a characteristic angular distribution of Rutherford scattering: $\frac{dN}{d\cos\theta^*} \sim (1 - \cos\theta^*)^{-2}$. The measured $\cos\theta^*$ distribution by the DØ Collaboration for the dijet mass range $175 < M_{jj} < 350$ GeV is shown in Figure 1(a) together with the LO and the NLO [4] QCD predictions. An additional cut, $\eta_{\text{boost}} = \frac{1}{2}(\eta_1 + \eta_2) < 2.0$, is applied in order to limit the

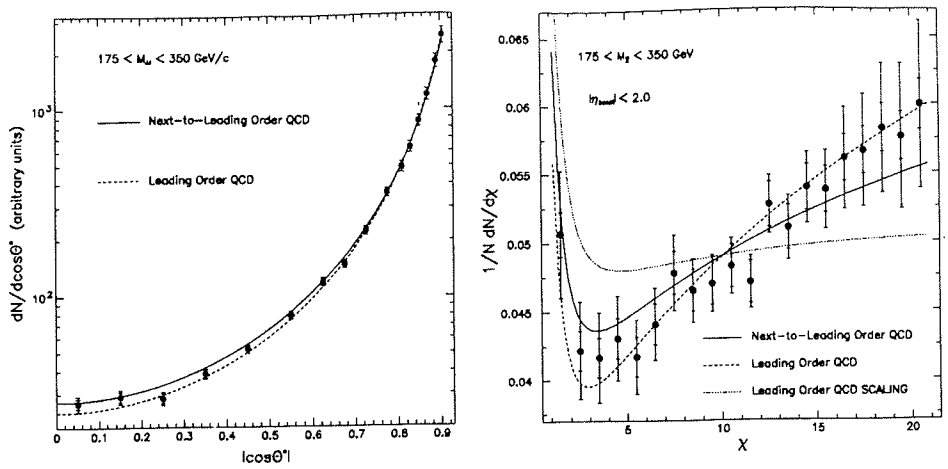

Figure 1: Dijet angular distributions measured by DØ: (a) $\frac{1}{N} \cdot \frac{dN}{d|\cos\theta^*|}$ and (b) $\frac{1}{N} \cdot \frac{dN}{d\chi}$ compared with LO and NLO QCD predictions.

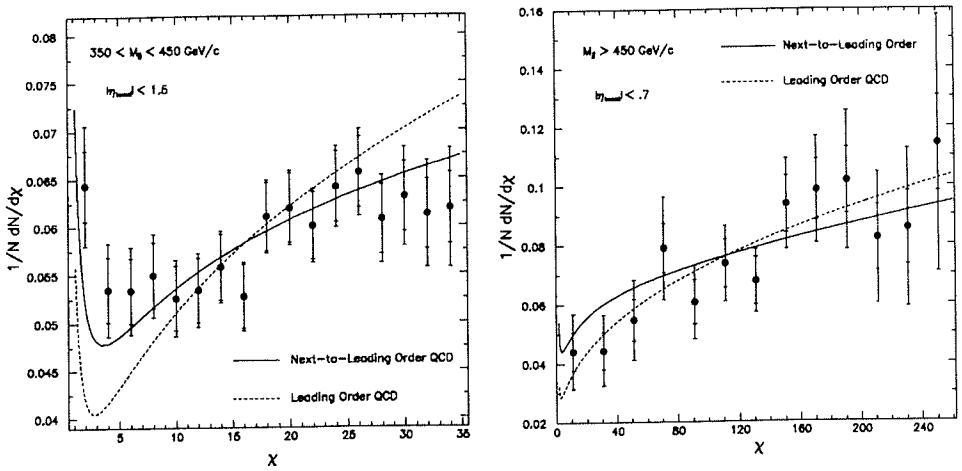

Figure 2: The measured $\frac{1}{N}\frac{dN}{d\chi}$ distributions by DØ for (a) $350 < M_{jj} < 450$ GeV and (b) $M_{jj} > 450$ GeV compared with LO and NLO QCD predictions.

jets to regions of good acceptance in the detector. Here η_1 and η_2 are pseudorapidities of the two jets. All distributions are normalized to unity. The presence of the pole at $\cos\theta^* = 1$ makes $\frac{1}{N}\frac{dN}{d|\cos\theta^*|}$ distribution unsuitable for a detailed comparison between the measurement and the QCD calculations. Thus, the χ variable defined by $\chi = e^{2|\eta^*|}$ is introduced, where η^* is the pseudorapidity in CMS frame: $\eta^* = \frac{1}{2}(\eta_1 - \eta_2)$. The χ variable transforms a $(1 - \cos\theta^*)^{-2}$ spectrum into a flat distribution. The same data is plotted in Figure 1(b) as a function of χ. Both the LO and NLO QCD calculations are seen to agree well with the data, where the CTEQ1M [5] parton distribution is used to derive the theoretical predictions. The QCD predictions for a constant α_s is also shown. The disagreement between data and the constant α_s prediction provides an indirect evidence for the running of α_s.

The study can be extended to large χ value by examining the distribution for events with large dijet masses. Figure 2 shows the $dN/d\chi$ distributions for dijet mass range (a) $350 < M_{jj} < 450$ GeV and (b) $M_{jj} > 450$ GeV. The disagreement between the data and the leading-order QCD curve is clearly visible in Figure 2(a). Figure 2(b) extends the reach in χ to 250, but the poor statistics do not allow us to distinguish between LO and NLO QCD calculations. This

study extends the range in χ over that previously published by CDF [6].

2.2 Dijet Differential Cross Sections

The dijet differential cross section $d^3\sigma/dE_T d\eta_1 d\eta_2$ is directly mapped to $d^3\sigma/dE_T dx_1 dx_2$ since: $x_1 = \frac{E_T}{\sqrt{s}}(e^{\eta_1} + e^{\eta_2})$ and $x_2 = \frac{E_T}{\sqrt{s}}(e^{-\eta_1} + e^{-\eta_2})$, Therefore, $d^3\sigma/dE_T d\eta_1 d\eta_2$ is sensitive to structure functions, especially to the gluon structure functions. In principle, with the availability of the NLO calculation, the gluon structure function can be extracted.

Both CDF and DØ have measured the differential cross section distribution. The measured $d^3\sigma/dE_T d\eta_1 d\eta_2$ as a function of E_T for $0.1 < |\eta_1| < 0.7$ and different $|\eta_2|$ slices by CDF are compared with the leading order QCD calculations in Figure 3(a). The $d^3\sigma/dE_T d\eta_1 d\eta_2$ distribution for $45 < E_T < 55$ GeV and $0.0 < |\eta_1| < 0.5$ as a function of $|\eta_2|\text{sign}(\eta_1 \cdot \eta_2)$ measured by DØ is plotted in Figure 3(b). For both figures, the QCD calculations are evaluated at renormalization scale E_T and the Morfin-Tung LO parton distributions [7] are used. The theory is normalized to the data. The theoretical predictions do not reproduce the shape of the data distributions well. While this might be attributed to a lack of knowledge of the low-x parton density functions, the difference is more likely due to next-to-leading order corrections.

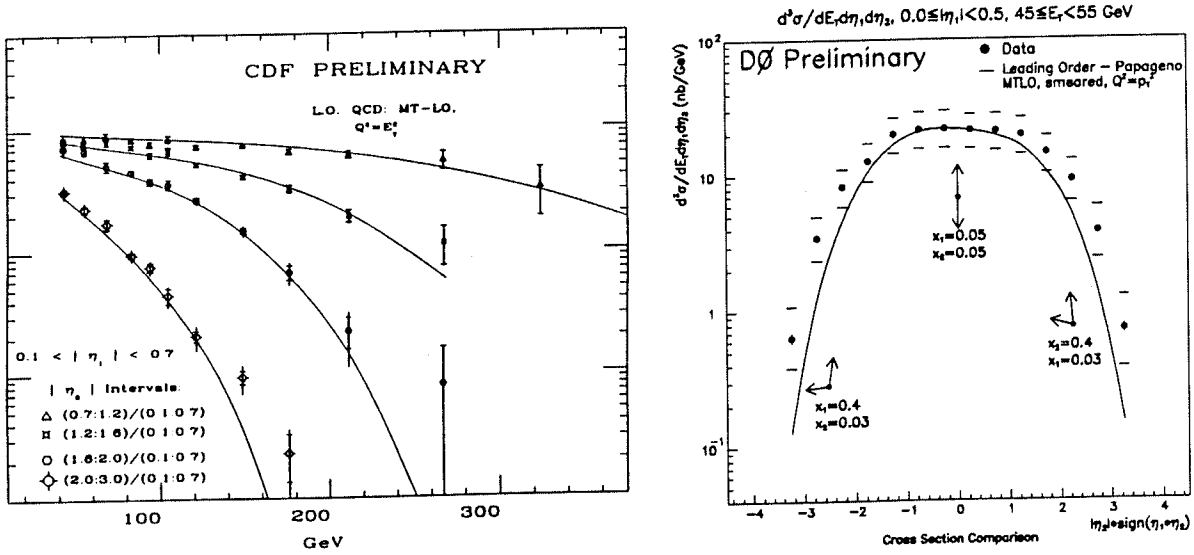

Figure 3: Dijet differential cross section (a) $d^3\sigma/dE_T d\eta_1 d\eta_2$ distributions as a function of E_T for different $|\eta_2|$ slices measured by CDF and (b) $d^3\sigma/dE_T d\eta_1 d\eta_2$ distribution as a function of $|\eta_2|\text{sign}(\eta_1 \cdot \eta_2)$ for $|\eta_1| < 0.5$ and $45 < E_T < 55$ GeV measured by DØ. The leading order QCD calculations are also shown.

2.3 Dijet Production for Different Rapidity Intervals

Recent theoretical calculation [8] studies dijet production with a large rapidity interval. The calculation resums all contributions to the cross section from intermediate "mini-jets", thus giving an approximation to all orders. The calculation predicts that as the rapidity distance between two jets increases, the correlation in jet E_T vanishes as demonstrated in Figure 4(a). The DØ collaboration has measured the dijet cross section as a function of E_T of the second jet for different rapidity intervals. The analysis requires the transverse energy of the first jet to be within the range $50 < E_T^1 < 55$ GeV. In addition, the average pseudorapidity ($\eta_{\text{boost}} = \frac{1}{2}(\eta_1 + \eta_2)$) of the two jets must be less than 0.5. The data are shown in Figure 4(b). The feature of vanishing E_T correlation as rapidity separation increases is well demonstrated in the data, although the direct comparison between the data and the prediction is not possible at the moment.

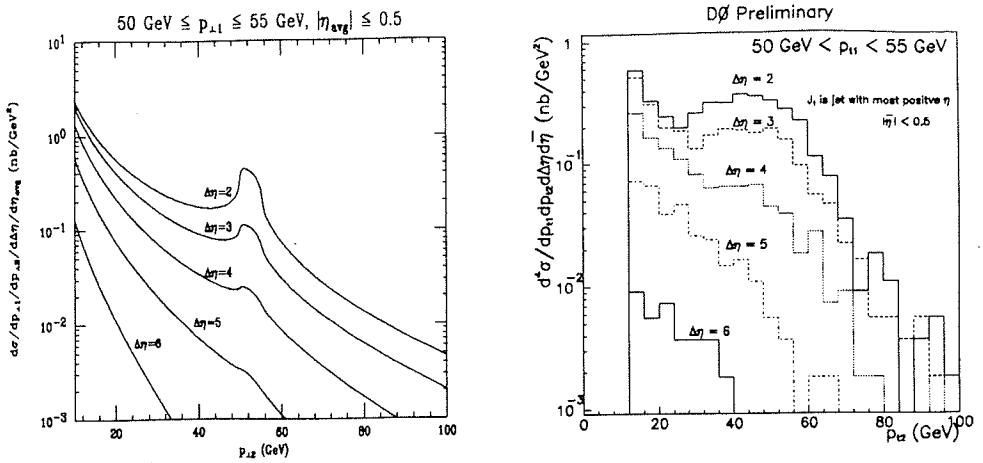

Figure 4: Dijet production cross section as a function of the E_T of the second jet for different rapidity separations (a) theoretical prediction and (b) the measured cross section by DØ.

3 Multijet Final States

Studies of multijet events allows the test of the validity of QCD calculations to higher order (α_s^3 or beyond). Recent analyses on the properties of multijet events are described below.

3.1 Topologies of Three-jet Events

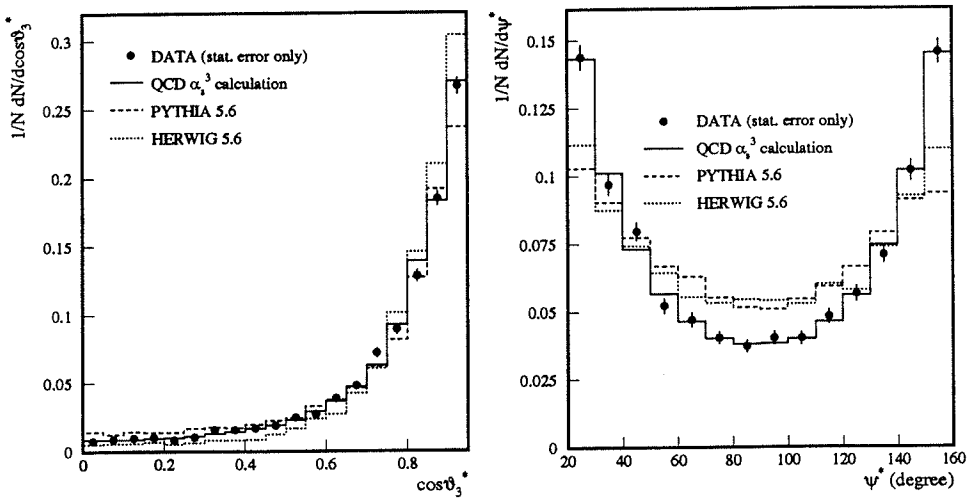

Figure 5: The measured three-jet angular distributions by DØ: (a) $\cos\theta_3^*$ and (b) ψ^* angle. The $\mathcal{O}(\alpha_s^3)$ QCD calculations and the predictions of the parton shower based Monte Carlo models are also shown.

Topological distributions for three-jet events have been published previously by UA1, UA2 and CDF [9]. DØ has performed a study with a higher statistics data sample and extended the study to previously untested regions of phase space of the topological distributions. In the three-jet center-of-mass system, the topologies of three-jet events are completely determined by four variables: the scaled energies of the leading jet ($x_3 = \frac{2E_3}{\sqrt{\hat{s}}}$) and the next-leading jet ($x_4 = \frac{2E_4}{\sqrt{\hat{s}}}$), the cosine ($\cos\theta_3^*$) of the polar angle of the leading jet and the angle (ψ^*) between the plane defined by the leading jet and the beam line and the plane defined by the two non-leading jets. Here E_3 and E_4 are the leading and next-leading jet energies in the CMS frame

and $\sqrt{\hat{s}}$ is the subprocess center-of-mass energy. The jets are required to have $E_T > 20$ GeV, $|\eta| < 3.0$ and $\Delta R > 1.4$ between jets. The highest jet E_T and the mass of the three jets must be greater than 60 GeV and 250 GeV, respectively. The following additional cuts are applied to select three-jet events: $x_3 < 0.9$, $\cos\theta_3^* < 0.95$ and $20° < \psi^* < 160°$. The DØ-measured $\cos\theta_3^*$ and ψ^* distributions are compared with the exact tree level calculations as obtained from the PAPAGENO program [10] and with the predictions of parton shower based Monte Carlo models in Figure 5. In general, the tree level QCD calculations are found to be in good agreement with the data while the parton shower based HERWIG [11] and PYTHIA [12] Monte Carlo models fail to provide a satisfactory description of the measured ψ^* distribution. The details of this analysis is reported in [13].

3.2 Properties of Multijet Events with Large Total Transverse Energies

CDF has studied the properties of multijet events with the scalar sum of the transverse energy greater than 420 GeV. The jets are selected by requiring $E_T > 20$ GeV, $|\eta| < 3.0$ and $\Delta R > 1.0$. The $\cos\theta^*$ of the event defined by $\cos\theta^* = \sqrt{1 - \frac{420^2}{\hat{s}}}$ is required to be less than 0.67 to ensure that events are well contained in the detector. The measured jet multiplicity distribution is compared with the HERWIG prediction in Figure 6(a). HERWIG gives a good description of the fraction of events with up to five jets. Figure 6(b) shows the measured ψ^* distribution for three-jet events with $M_{jjj} > 500$ GeV, $x_3 < 0.9$ and $|\cos\theta_3^*| < 0.6$. Again HERWIG prediction agrees with the data. It is worth noting that the phase space explored in Figure 6(b) is very different from that explored in Figure 5(b). In conclusion, CDF found that the angular, mass, jet multiplicity and jet transverse momentum distributions of events with large total transverse energy are well described by the HERWIG Monte Carlo program. The analyses are summarized in [14].

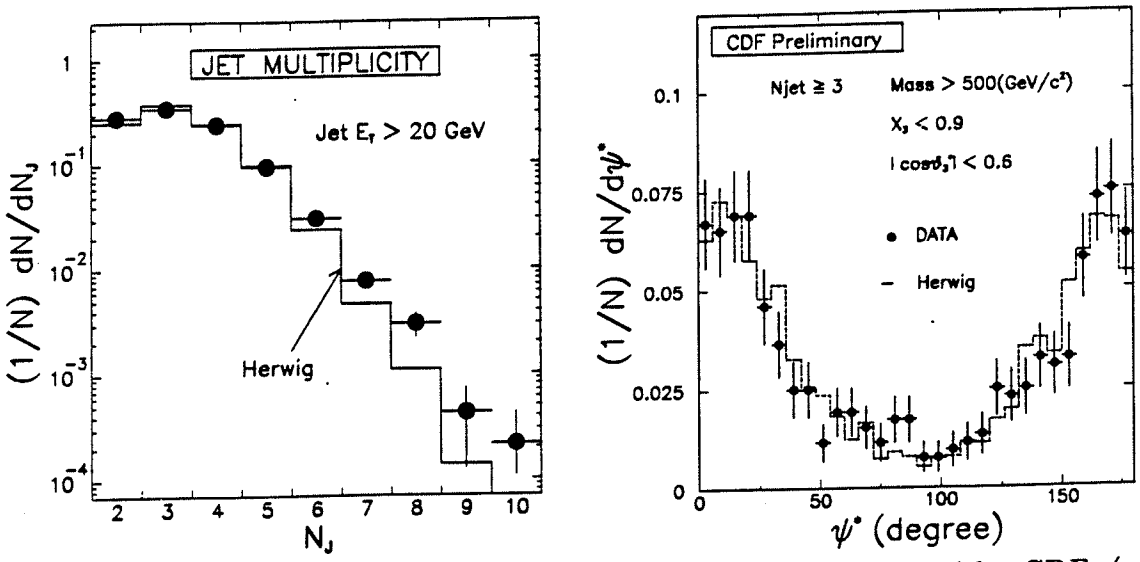

Figure 6: Properties of multijet events with $\Sigma E_T > 420$ GeV measured by CDF: (a) jet multiplicity distribution and (b) the ψ^* distribution of inclusive three-jet events.

4 Rapidity Gap Events

Rapidity gaps are regions of rapidity containing no particles. They are typically associated with low transverse momentum processes such as elastic and diffractive scattering. At high energies, they are also expected from processes when a color singlet is exchanged between interacting partons [15]. A rapidity gap will not be observed in the final state, however, if spectator interactions produce particles between the jets. While both the cross section for producing a rapidity gap from the hard scattering (σ_{gap}) and the probability of the gap surviving spectator

interactions (S) are of theoretical interest, experiments are only directly sensitive to the product of these factors. An experimentally accessible quantity is the fraction of events with a rapidity gap between the two leading jets defined by: $f(\Delta\eta) = \frac{\sigma_{gap}(\Delta\eta)\cdot S(\Delta)}{\sigma(\Delta\eta)}$.

The DØ Collaboration has obtained the first experimental information on the rapidity gap fraction. The electromagnetic section of the calorimeters is used to search for rapidity gaps. A particle is tagged by the deposition of more than 200 MeV transverse energy in an EM calorimeter tower. The measured fraction of rapidity gap events as a function of gap width is shown in Figure 7(a). This detector-dependent measurement can be used to obtain an upper limit on the fraction of events with no particles between jets. The upper limit on the rapidity gap fraction for $\Delta\eta_c > 3$ is $f(\Delta\eta_c > 3) < 1.1 \times 10^{-2}$ at 95% C.L. This limit constrains the product of σ_{gap}/σ and S for $\Delta\eta_c > 3$ as shown in Figure 7(b). The details of the analysis can be found in [16].

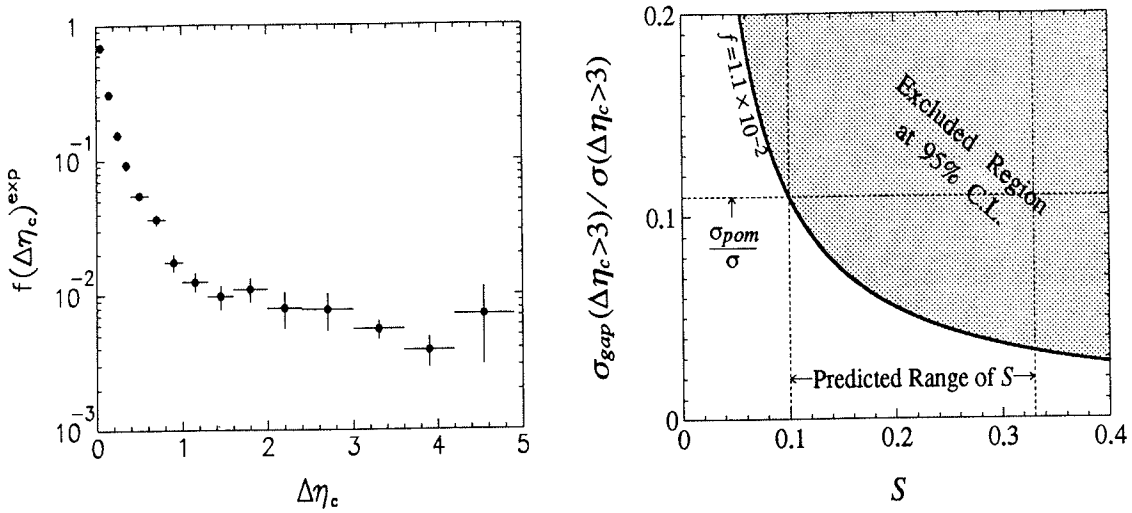

Figure 7: (a) The fraction of events that have no tagged particles between two leading jets as a function of $\Delta\eta_c$ measured by DØ. (b) The limit on $\sigma_{\rm gap}/\sigma$ versus S for $\Delta\eta_c > 3$.

5 Summary

Both CDF and DØ have studied the dijet and multijet final states in detail. The large coverage of the DØ calorimetry allows studies of events in the forward region and events with large rapidity separations. The measured dijet angular distributions, dijet differential cross sections, and dijet production for different rapidity separations are compared with either the leading-order or the next-leading-order QCD calculations. Generally, the calculations are found in good agreement with the data. The properties of multijet events are compared with those of QCD calculations and of parton shower Monte Carlo models. The QCD calculations describe the data well. DØ has searched for events with a rapidity gap between jets. The result provides a significant constraint on the theoretical gap fraction as a function of the survival probability. With the even larger data sample expected from the on-going and future Tevatron runs, both experiments will continue carrying out more detailed studies of dijet and multijet final states.

Acknowledgement

I wish to express my gratitude to A. Brandt, M. Fatyga, B. Flaugher and D. Koltick for reviewing of my presentation and/or critical reading of this write-up. I would also like to thank A. Brandt, J. Blazey, B. Flaugher, S. Geer, T. Geld, R. Harris, T. Heuring, A. Milder, R.

Plunkett and H. Weerts for providing results and plots on which this write-up is based.

References

[1] M. Gell-Mann, *Acta Physica Austria*, Suppl. **IX** (1972) 733;
H. Fritzsch and M. Gell-Mann, 16th International Conference on High Energy Physics, Batavia, 1972, editors J.D. Jackson and A. Roberts, National Accelerator Laboratory (1972);
H. Fritzsch, M. Gell-Mann and H. Leytwyler, Phys. Lett. **B47** (1973) 365.

[2] CDF Collaboration, F. Abe *et al.*, NIM **A271** (1988) 383;
DØ Collaboration, S. Abachi *et al.*, NIM **A338** (1994) 185.

[3] UA1 Collaboration, G. Arnison *et al.*, Phys. Lett. **B132** (1983) 214.

[4] S. Ellis, Z. Kunszt and D. Soper, Phys. Rev. Lett., **64** (1990) 2121.

[5] J. Botts *et al.*, Fermilab preprint, FERMILAB-Pub-92/371.

[6] CDF Collaboration, F. Abe *et al.*, Phys. Rev. Lett. **69** (1992) 2896.

[7] J.G. Morfin and W.K. Tung, Z. Phys. **C52** (1991) 13.

[8] V. Del Duca and C. Schmidt, DESY preprint 93-139/SCIPP 93/35.

[9] UA1 Collaboration, G. Arnison *et al.*, Phys. Lett. **B158** (1985) 494;
UA2 Collaboration, J.A. Appel *et al.*, Z. Phys. **C30** (1986) 341;
CDF Collaboration, F. Abe *et al.*, Phys. Rev. **D45** (1992) 1448.

[10] I. Hinchliffe, "The PAPAGENO Partonic Monte Carlo Program", LBL preprint, LBL-34372.

[11] HERWIG 5.6 Program:
G. Marchesini and B. Webber, Nucl. Phys. **B70** (1974) 93;
I.G. Knowles, Nucl. Phys. **B310** (1988) 571;
G. Marchesini *et al.*, Comp. Phys. Comm. **67** (1992) 465.

[12] PYTHIA 5.6 Program:
H.U. Bengtsson and T. Sjöstrand, Comp. Phys. Comm. **46** (1987) 43.

[13] J. Qian, "A Test of QCD Based on the Topologies of the Three- and Four-Jet Events", DØnote #1868 (1993).

[14] CDF Collaboration, F. Abe *et al.*, Phys. Rev. **D145** (1992) 2249;
S. Geer, CDF note CDF/JET/DOC/CDFR/2443 (1994);
T. Asakawa and S. Geer, CDF note CDF/JET/DOC/CDFR/2449 (1994).

[15] Y. Dokshitzer, V. Khoze and S. Troyan, Proceedings of the 6th International Conference on Physics in Collisions (1986), editor M. Derrick, World Scientific, Singapore (1987);
J.D. Bjorken, Phys. Rev. **D47** (1992) 101.

[16] DØ Collaboration (S. Abachi *et al.*), Phys. Rev. Lett., **72** (1994) 2332.